Preprint Version

Data Sampling Schemes for Microstructure Design with Vibrational Tuning Constraints

Arindam Paul[1,a], Pinar Acar[2,b], Ruoqian Liu[1,c], Wei-keng Liao[1,d], Alok Choudhary[1,e], Veera Sundararaghavan[2,f], Ankit Agrawal[1,g]
[1]*Northwestern University, Evanston, IL, 60208*
[2]*University of Michigan, Ann Arbor, MI, 48109*

Microstructures significantly impact the performance of sensitively engineered components, such as wireless impact detectors used in military vehicles or sensors used in aircrafts. These components can operate safely only within a certain range of frequencies, and frequencies outside that range could lead to instability because of resonance. This paper addresses optimization of microstructure design to maximize the yield stress of a Galfenol beam under vibration tuning constraints defined for the first torsional and bending natural frequencies by using a data-driven solution scheme. In this study, two carefully designed algorithms are used to sample the entire microstructure space.

Classical optimization techniques often lead to a unique microstructural solution, rather than yielding the complete space of optimal microstructures. Multiple optimal solutions are imperative for the practicality of design as conventional low-cost manufacturing processes can generate only a limited set of microstructures. Our data sampling-based methodology outperforms or on par with other optimization techniques but also provides numerous near-optimal solutions, 2-3 orders of magnitude more than previous methods. Consequently, the proposed framework delivers a spectrum of optimal solutions in the microstructure space which can accelerate materials development and reduce manufacturing costs.

[a] Graduate Research Assistant, Department of Electrical Engineering and Computer Science, Northwestern University, Evanston, IL
[b] Research Fellow, Department of Aerospace Engineering, University of Michigan, Ann Arbor, MI, AIAA Student Member
[c] Graduate Research Assistant, Department of Electrical Engineering and Computer Science, Northwestern University, Evanston, IL
[d] Research Professor, Department of Electrical Engineering and Computer Science, Northwestern University, Evanston, IL
[e] Professor, Department of Electrical Engineering and Computer Science, Northwestern University, Evanston, IL
[f] Associate Professor, Department of Aerospace Engineering, University of Michigan, Ann Arbor, MI, AIAA Member
[g] Research Associate Professor, Department of Electrical Engineering and Computer Science, Northwestern University, Evanston, IL

Nomenclature

σ = volume averaged stress (in MPa)

ε = volume averaged strain

ω_{1b} = first bending natural frequency (in Hz)

ω_{1t} = first torsional natural frequency (in Hz)

α = constant

m = mass of the beam

J = torsion constant

E_1 = Young's modulus along axis-1 (in GPa)

G_{12} = shear modulus in 1-2 plane (in GPa)

I_1 = moment of inertia along axis-1

L = beam length

q = volume normalization vector

r = orientation

V = null space vector

t = time

S = compliance (in 1/GPa)

C = spacial correlation matrix

C_{eff} = effective stiffness vector

A = orientation distribution function

χ = orientation dependent property

Z = integers

ϵ = very small value

I. Introduction

One of the primary aims of materials science and engineering research is to understand the association between materials' processing, structure, properties, and performance [1–10]. It is recognized that even for a particular alloy system, variability in microstructure leads to a wide range of materials properties, and it substantially impacts the materials' performance, especially under extreme conditions. Thus, optimization of the microstructure can significantly improve the materials' performance. It is even more pertinent for sensitively engineered components that use magnetostrictive materials. Magnetostrictive materials undergo a change in shape or dimensions in response to a magnetic field. Further, such materials can respond to external stresses by altering their magnetic states. The state of the art of magnetostrictive materials and their applications in a large variety of engineering applications was discussed by Olabi and Grunwald [11]. The authors also showed improvement in material features with the use of magnetostrictive materials. The magnetostrictive properties of different materials such as cubic Laves phases such as TbFe2, Terfenol D, and SmFe2, as well as Fe-X alloys based on Fe-Ga and Fe-Al, were presented by Grossinger et al. [12]. The design of magnetostrictive actuators and transducers has been discussed in literature [11, 13–15]; however, the design of microstructural properties of magnetostrictive materials has not been studied extensively yet. Galfenol is one such example of a magnetostrictive material [16, 17]. It has been widely used in aerospace applications as a sensor material in beam shaped structures. Galfenol can be processed using conventional rolling and wire drawing equipment, and it can be machined using conventional mills and lathes, and welded to a wide array of materials. The potential of Galfenol to develop desired anisotropic properties and flexibility regarding processing makes it a lucrative material. The single crystals of Galfenol material can provide large magnetostriction; however, their preparation is expensive. It is possible to develop comparable polycrystalline textured Galfenol material as expensive single crystals by applying thermomechanical processes such as rolling and extrusion [18–20]. However, control and prediction of the large changes in properties such as magnetostriction and yield strength during thermomechanical processing can be difficult. For instance, warm rolled and annealed specimens retain high magnetostriction but are quite brittle; whereas, cold rolled specimens have high yield strength but lose their magnetostriction [21, 22]. Experimental studies suggest that internal inhomogeneous strains introduced by microstructural changes play a major role in determining the final magnetostriction in Galfenol [23]. The computation of magnetostrictive strain of a polycrystalline

Galfenol material was studied before by Kumar and Sundararaghavan [17].

The orientation distribution function (ODF) is used to represent the microstructure. The ODF represents the volume fractions of the crystals of different orientations in the microstructure. The complete range of properties obtainable from the space of ODFs is represented using property closures, approximated by the space defined with either upper or lower bound of a given property [16]. Upper bound closure of stiffness values represents the range of properties obtainable by the upper bound homogenization relation while a lower bound closure of compliance values shows the properties obtainable by the lower bound homogenization equation. An approach that is gaining popularity in new materials development is selective optimization of certain properties of a material in a particular direction or plane while sacrificing the properties across other directions or planes that are not as important for the design problem [24].

There have been few efforts to optimize the microstructure to satisfy a given set of desired properties. Liu et al. [25] achieved this by directly sampling the ODF space using a data mining methodology. Some researchers have adopted sampling within the property hull and use a Fourier basis for discretizing the ODF [26–28]. In [16, 29], Acar et al. derived an upper bound solution approach starting with generating samples in the space of macro elements (Young's modulus and shear modulus parameters) and then identified multiple optimal solutions through a linear solver. Acar et al. in [24] formulated a Linear Programming (LP) solution based method for constructing property closures (for the homogenization relations considered here) by establishing the smallest convex region enveloping single crystal property points.

However, all these approaches used for constrained microstructure optimization lead to only one or in some cases, a handful of solutions. Further, the process for obtaining multiple solutions is often a trial and error based method. On the other hand, conventional and economical manufacturing processes, such as metal forming and heat treatment can generate only a limited set of microstructures [21, 23, 30]. Moreover, it may not be economically feasible to manufacture a single design solution [3]. Thus, there is a big incentive for developing approaches that can conceive a spectrum of optimal structures.

The paper proposes a data sampling based scheme to find numerous near-optimal microstructures to maximize yield stress given vibrational design constraints. The proposed framework involves developing and executing sampling algorithms to generate possible ODF solutions satisfying the process limitations. The sampling algorithms developed in this work, *partition* and *allocation* schemes, are complementary to one

another and ensure sampling of the entire feature space. Data points satisfying both the bending and torsional frequency constraints are generated. The proposed data sampling methodology outperforms (or on part with) other optimization techniques and provides 2-3 order of magnitude more near-optimal solutions. Further, our approach opens up additional opportunities for reducing the dimensionality of microstructure space to accelerate the process of achieving solutions that satisfy all the constraints by isolating ODF dimensions that are non-zero across a majority of near-optimal ODF solutions. The solution methodology presents an extensive approach, and thus it can be applied to different ODF representations such as finite element discretization and Fourier series expansion.

The rest of the paper is organized as follows. Section II provides a brief background of microstructure, orientation distribution function and Galfenol alloy. Section III discusses some related works on the optimization of microstructure design for polycrystalline metals. Section IV describes the vibration tuning problem, and Section V presents the proposed data sampling-based methodology for optimization. In Section VI, the results are discussed and examined, and finally, Section VII presents the conclusion and offers some recommendations for future studies.

II. Background

A. Property representation in Rodrigues' space

The alloy microstructure consists of multiple crystals where each crystal has its distinct orientation. The ODF represents the volume fractions of the crystals of different orientations in the microstructure. The microstructure of the Galfenol alloy system in this work is modeled using ODFs [31–34] which are represented by axis-angle parameterization of the orientation space, as proposed by Rodrigues [35]. Angle-axis representations elucidate an alternate way of representing orientations compared to Euler angles. The Rodrigues' parameterization is created by scaling the axis of rotation n as $r = ntan\frac{\theta}{2}$, where θ is the rotation angle.

The ODF, a primary concept in texture analysis and anisotropy, is defined based on a parameterization of the crystal lattice rotation. Orientation distributions can be described mathematically in any space appropriate to a continuous description of rotations [31, 32, 35]. The orientation space can be reduced to a subset called the fundamental region, as a consequence of crystal symmetries. Each crystal orientation is depicted uniquely inside the fundamental region by a parameterization coordinate for the rotation r. The ODF, represented

by $A(r)$, is the volume density of crystals of orientation r. The fundamental region is discretized into N independent nodes with N_{elem} finite elements and N_{int} integration points per element. A detailed explanation of the ODF discretization and volume averaged equations has been provided in [16, 24, 25, 29]. A single particular orientation or texture component is represented by each point in the orientation distribution. The orientation distribution information can be used to determine the presence of components, volume fractions and predict anisotropic properties of polycrystals. Although the term distribution function is used for ODFs, this is distinct from "distribution function" used for cumulative frequency curve in statistics. The ODF is a probability density but is constrained such that it is normalized to unity over the fundamental region. Figure 1 represents the finite element discretization of the orientation space of BCC Galfenol.

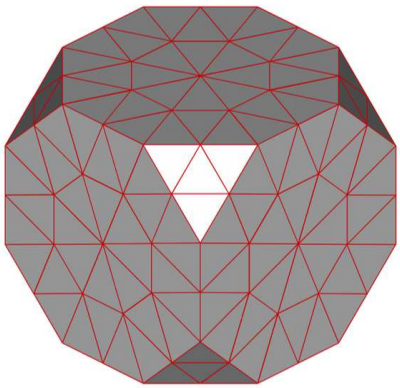

Fig. 1: Finite element discretization of the orientation space of BCC Galfenol

The microstructure of an alloy is comprised of multiple crystals, and each crystal has an orientation. The generalized Hooke's law for the agglomeration is expressed as:

$$< \sigma_{ij} >= C^{eff}_{ijkl} < \varepsilon_{kl} > \tag{1}$$

ε_{kl} and σ_{ij} represent the volume-averaged strain and yield stress of the agglomeration. C^{eff}_{ijkl} represent the tensor for effective stiffness in the given coordinate system. C^{eff} is the average over aggregate of the crystals [24, 36] where $< C >$ represents stiffness tensor for each crystal.

$$C^{eff} =< C > \tag{2}$$

The averaging is performed over an aggregate of the crystal in a macro-scale elementary volume. Crystal size and shape are ignored, and homogeneous deformity is assumed. The ODF represents the volume density of

each orientation in the microstructure. $\chi(r)$ represents the orientation dependent property for single crystals and $< \chi >$ depicts the expected value.

$$< \chi >= \int_R \chi(r) A(r,t) dv \tag{3}$$

Using this parametrization, any polycrystal property can be expressed in a linear form as follows, where $A(r_m)$ is the value of the ODF at the m^{th} integration point with global coordinate r_m of the n^{th} element, $|J_n|$ is the Jacobian determinant of the nth element, w_m is the integration weight associated with the m^{th} integration point, and $\frac{1}{(1+r_m.r_m)^2}$ represents the metric of Rodrigues parameterization.

$$< \chi >= \chi(r) A(r,t) dv = \sum_{n=1}^{N_{elem}} \sum_{m=1}^{N_{int}} \int_R \chi(r_m) A(r_m) w_m |J_n| \frac{1}{(1 + r_m.r_m)^2} \tag{4}$$

A (which symbolizes the ODF) is a function of orientation r and time t during processing that satisfies the following normalization constraint :

$$\int_R A(r,t) dv = 1 \tag{5}$$

The complete range of properties obtainable from the space of ODFs is represented using property closures, approximated by the space between upper and lower bound of the given property [16].

$$< C >= \int_R CA dv \tag{6}$$

The upper bound homogenization relation (above) is based on the assumption of constant strain throughout the thickness of the beam and is represented by the upper bound closure of stiffness values. The upper bound average or the Voigt average [37] is calculated by averaging the particular property (in this case, stiffness) by multiplying the ODF vector with the property vector. However, the lower bound approach (below) is based on the assumption of constant stress throughout the plate thickness. For the lower bound average or the Reuss average [37], the inverse of the given property is averaged. For instance, in the equation below, compliance (C^{-1} or S), the inverse of stiffness, is averaged by using the lower bound approach and the equation is written for the compliance matrix. $< C >$ and $< C^{-1} >$ represent the volume-averaged macroscopic stiffness formulation in C and C^{-1} space. C^{-1} refers to compliance.

$$< C^{-1} >= \int_R C^{-1} A dv \tag{7}$$

The yield stress is computed for the upper and lower bound approaches in terms of single crystal yield strengths along the beam axis as follows:

$$< \sigma_y >= \int \sigma_y A dv \tag{8}$$

$$< \sigma_y^{-1} >= \int \sigma_y^{-1} A dv \tag{9}$$

B. BCC Galfenol

Galfenol is a general name for an iron-gallium alloy, and the name was first associated in 1998 when it was discovered that adding gallium to iron increases its magnetostrictive effect [38, 39]. A magnetostrictive material is used to harvest vibrational energy because of its property to change shape in response to a magnetic field. Galfenol also responds to external stresses by altering its magnetic state [40]. Researchers have found Galfenol to demonstrate magnetostrictive strains of up to 400 ppm in single crystal form (which is more than ten times that of α-Fe [25]). Moreover, processing Galfenol does not need any customized equipment. It can be processed using conventional rolling and wire drawing equipment, and it can be machined using standard mills and lathes, and can also be welded to a variety of materials [41]. Galfenol converts applied mechanical energy with high efficiency (around 70 percent) into magnetic energy and vice versa [42]. Researchers have found that groups of contorted cells respond to a magnetic field by rotating their magnetic moments to align with the field which in turn, changes the exterior dimensions of the crystal. This contortion from the α-Fe structure is responsible for Galfenol's superior performance [43]. Adding gallium generates imperfections in iron's otherwise orderly lattice thus improving the magnetostrictive property of the resultant alloy [44]. Single crystals of Galfenol impart large magnetostriction, but the preparation of monocrystal Galfenol is expensive. Hence, there is an impetus for the development of polycrystalline Galfenol with favorable properties for various design problems [21, 23, 30]. Figure 2 (a) represents the polycrystalline microstructure of Galfenol, with different colors representing different crystal orientations. For this BCC structure, the Rodrigues fundamental region includes 76 independent nodal points (ODF values) as shown in Fig. 2 (b). It is to be noted that the red nodes in Fig. 2 (b) are indicating the 76 independent ODF values, and the ODF values of the blue nodes can be computed using the crystallographic symmetries.

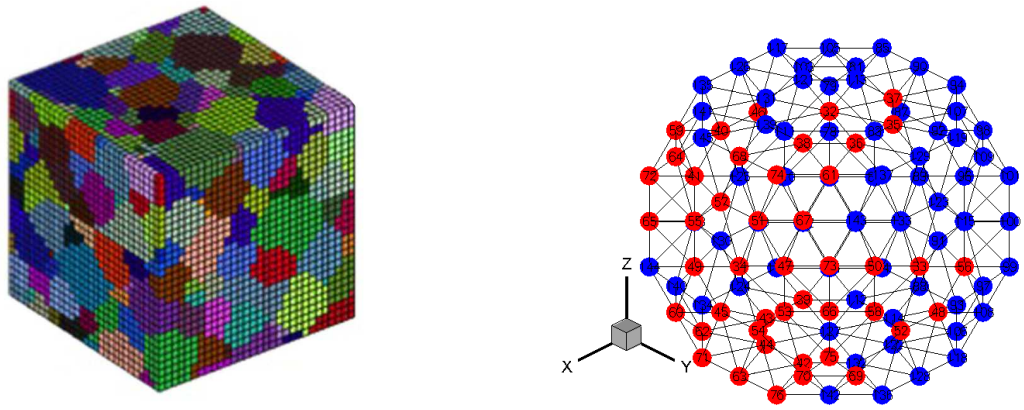

(a) BCC Galfenol microstructure

(b) ODF representation indicating the location of 76 independent nodes in the orientation space in red

Fig. 2: Finite element discretization of the orientation space of BCC Galfenol

Among potential applications, Galfenol has a wide application area in aerospace as it is usually used as a sensor material in beam shaped structures. Moreover, electromagnetic waves travel three orders of magnitude faster than mechanical waves [42] with the impact information transmitted ahead of the waves created by the impact, and researchers have found that different configurations of Galfenol energy harvesters can provide power to operate remote sensors and radios [45]. The presence of high stiffness [46], magnetostrictive strains [47, 48], and yield strength [49] together makes Galfenol ideal for actuators [50] in cantilever beam devices to generate sonar waves, or as sensors for measuring vibrations, or as energy harvesting devices to produce electricity [25].

III. Related Works

Liu et al. [25, 51] used a combination of random sampling and feature selection for the purpose of optimization of multiple design objectives, using guided and generalized pattern search. Pattern search [52–55] finds a sequence of points, $x_0, x_1, x_2, \ldots$, called a mesh, that approaches an optimal point by computing a sequence of points. The mesh is constructed by adding a starting point to a scalar multiple of a set of vectors. Once the pattern search algorithm identifies a point in the mesh that enhances the objective function at the new point, this point becomes the new optimal point for the next step of the algorithm. The current problem

is more convoluted as compared to Liu et al.'s due to additional constraints on the first natural frequencies. These constraints make the problem much more complex and difficult to optimize using feature selection based methods. It is because the neighborhood of a valid solution is often rendered invalid due to not meeting the constraints.

The optimization of microstructure design of Galfenol vibration tuning problem with constraints has been studied earlier in [16, 24, 29]. In [16, 29], the optimization problem was defined to maximize the yield stress of a cantilever beam under vibration tuning constraints. The authors derived an upper bound solution approach starting with generating samples in the space of macro elements (Young's modulus and shear modulus parameters) and then identifying the multiple optimal solutions through a genetic algorithm based solver. The linear solver scheme used a sampling technique called Incremental Space Filler (ISF) [56]. The ODFs for every global value was computed using ISF, and subsequently, the highest value of the yield stress among the feasible solutions was searched. Acar et al. in [24] formulated a Linear Programming (LP) [57] solution approach method for constructing property closures (for the homogenization relations considered here) by establishing the smallest convex region enveloping single crystal property points. LP is a rigorous and intuitive approach for the construction of property closures as closures are obtained as a result of property maximization or minimization. Connecting faces on the closure may contain polycrystals explicitly identified by the LP approach, which is well-suited for other problems, such as identification of textures with desired property combinations where several properties are optimized simultaneously. The authors augmented the initial solution with null space to attain multiple solutions. However, the LP approach has few limitations. First, a LP method can be implemented only when the original non-linear problem can be adapted to a linear problem. In addition, unlike the data sampling-based schemes proposed in this work, there is a limited number of multiple solutions possible. Further, the procedure to obtain the multiplier to the null space is determined by trial-and-error. The advantage of a data sampling based methodology is that it can explore the neighborhood of the optimal solution and generate many near-optimal solutions.

IV. Problem Description

We aim to explore the microstructure design constraint of a cantilevered Galfenol beam for a vibration tuning problem with yielding objective. The vibration tuning puts a restriction on the ODF solutions to have a finite number of directions in the solution space. The number of independent ODF values is 76 at this time

since Galfenol has a BCC structure [25]. The design objective is determined as the maximization of yield stress while the first bending and torsional frequencies are constrained for vibration tuning. The primary goal of the problem is to find the best microstructure design that maximizes the yield stress of the beam and satisfies the given vibration constraints.

The rationale behind constraining the operating frequencies is to eliminate possible dynamic instabilities, for instance, in sensor materials in aircraft beams [58, 59]. The main goal of the problem is to find the best microstructure design that maximizes the yield stress of the beam and satisfies the given vibration constraints.

The torsional and bending frequency constraints are given by the following equations:

$$\omega_{1t} = \sqrt{\frac{G_{12}J}{\rho I_p}} \tag{10a}$$

$$\omega_{1b} = (\alpha L)^2 \sqrt{\frac{E_1 I_1}{mL^4}} \tag{10b}$$

$$\text{where } \alpha L = 1.87510 \tag{11}$$

Here $G_{12} = 1/S_{66}$, $E_1 = 1/S_{11}$, and S being the compliance elements ($S = C^{-1}$), E_1 being the Young's modulus along axis-1 and G_{12} being the shear modulus in 1-2 plane. In these formulations, J is torsion constant, ρ is density, I_p is polar inertia moment, m is unit mass, L is length of the beam and I_1 is moment of inertia along axis-1. The mathematical formulation of the optimization problem is given below:

$$\max \ \sigma_y \tag{12}$$

$$A \geq 0 \tag{13}$$

$$\int A dv = 1 \tag{14}$$

The optimization problem includes the unit volume constraint by definition (Equation 14). The other constraints are the first natural frequencies to tune the beam vibration. In this problem, the length of the

beam is taken as L=0.45 m, and the beam is considered to have rectangular cross section with dimensions a=20 mm and b=3 mm. The values of stiffness parameters for Galfenol single crystals are taken as C_{11} = 213 GPa; C_{12} = 174 GPa and C_{44} = 120 GPa [16, 24, 29]. C_{11}, C_{12}, C_{13} and C_{14} comprise the most dominant elements in stiffness matrix, a measure of the durability of a given material. The stiffness values of the polycrystal are computed using the upper bound averaging (C-space) while the lower bound (C^{-1}-space) computation provides the compliance parameters. Figure 3 depicts the geometric representation of Galfenol beam vibration problem. There are two sets of constraints presented below. Each set of constraint has a lower and upper bound on the torsional and bending frequencies.

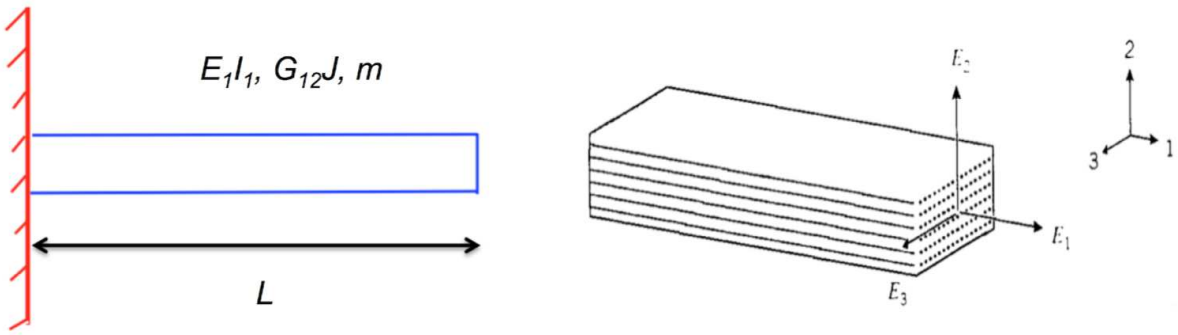

Fig. 3: Geometric representation of Galfenol beam vibration problem

First set of constraints:

$$\textit{subject to } 19.5 \text{ Hz} \leq \omega_{1t} \leq 21.5 \text{ Hz} \tag{15a}$$

$$\textit{subject to } 120 \text{ Hz} \leq \omega_{1b} \leq 122.5 \text{ Hz} \tag{15b}$$

Second set of constraints:

$$\textit{subject to } 21.5 \text{ Hz} \leq \omega_{1t} \leq 23.5 \text{ Hz} \tag{16a}$$

$$\textit{subject to } 100 \text{ Hz} \leq \omega_{1b} \leq 114 \text{ Hz} \tag{16b}$$

It is important to note that both sets of constraints are specimens, and factual constraints may differ based on the real material design. Nonetheless, they are representative of a real-world design problem for magnetostrictive materials where there are bounds on first natural frequencies.

V. Methodology

An overview of the proposed system is first presented and then the algorithms proposed for sampling the ODF space for the given problem are explained.

A. Overview of the System

The paper proposes a two-step data-driven solution scheme to find optimal microstructure satisfying performance requirements, and design and manufacturing constraints. The first phase of the approach involves developing and executing sampling algorithms to generate possible ODF solutions meeting the process limitations. The sampling algorithms i.e. *partition* and *allocation* scheme complement one another and ensure sampling the entire feature space. *Partition* warrants that different permutations of non-zero ODF dimensions are explored for a given set of ODF dimension. *Allocation* guarantees that all the ODF dimensions are explored sufficiently.

In the second step, data points are generated by satisfying both the bending and torsional frequency constraints. A future direction for reducing the dimensionality of microstructure space is highlighted that can accelerate the process of achieving solutions satisfying all the constraints by isolating ODF dimensions that are mostly non-zero across a majority of near-optimal ODF solutions. Figure 4 illustrates the steps in the proposed framework in a flow-diagram.

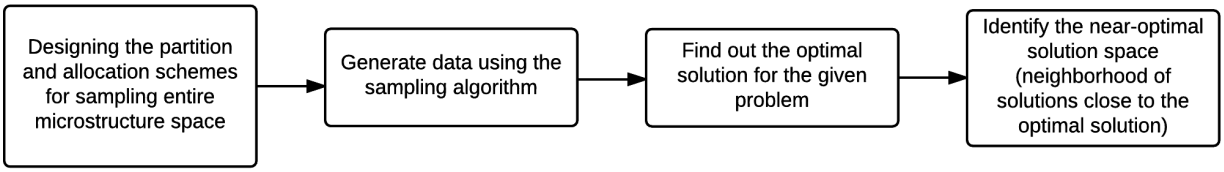

Fig. 4: Flow diagram of the proposed methodology. Upper and lower bound approaches for both sets of constraints are repeated for both problems.

B. Algorithms

Two sampling techniques *partition* and *allocation* algorithms developed in the proposed work are presented. The algorithms ensure to address the problem of sufficiently sampling the problem space and generate ODFs fulfilling the constraints in the problem objective.

1. Partition Method

In this method, the unit length is divided into k small segments, and k is decided by a limit set as D. D is the number of dimensions and in case of Galfenol, D is equal to 76. k-1 random cuts between the interval [0,1] (Figure 5) are made, where k is the number of non-zero ODF dimensions in the ODF vector. It is iterated from 1 to D-1 with an increasing number of samples generated with regards to k and then down sampled to 1000 for each iteration, except when k=1, D samples exist (corresponding to D single crystals) and are all used. The steps of the partition algorithm (pseudocode) are outlined below.

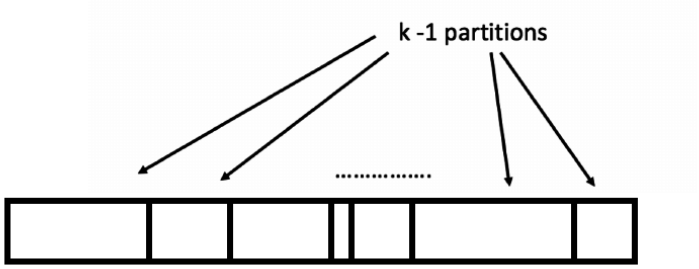

Fig. 5: Partition Algorithm : The unit length is divided into k small segments, and k is decided by a limit set as D. The algorithm iterates from 1 to D-1 with an increasing number of samples generated with regards to k and then down sampled to 1000 for each iteration.

2. Allocation Method

In this method, k values are randomly generated at a time. It continues only when the sum S is less than the whole (in this case 1). As mentioned above, the sum of the product of the volume fraction (vf) and density functions (df) across each dimension must add up to 1. The threshold is updated to the remainder 1 -

Algorithm 1 Partition algorithm

```
1: procedure PARTITION
2:     D ∈ Z
3:     for k ∈ {1, ..., D − 1} do
4:         for i ∈ {1, ..., 1000} do
5:             for cut ∈ {1, ..., k − 1} do
6:                 Make an arbitrary cut
7:             end for                          ▷ Sample with k cuts generated
8:         end for                              ▷ 1000 samples with different cuts
9:     end for
10:    return
11: end procedure
```

S and continues until this remainder is sufficiently small. k=1 is the trivial case where the product of the vf and df equals to 1. The steps of the allocation algorithm (pseudocode) are presented below.

Both the partition and allocation methods are based on the heuristic that in a valid microstructure obeying all the constraints, only a few of all the dimensions of the ODF vector is non-zero. However, these

Algorithm 2 Allocation algorithm

```
1: procedure ALLOCATION
2:     Generate a random k ∈ {1, ..., 76}
3:     Sum ← 0
4:     for i ∈ {1, ..., k} do
5:         Sum ← Sum + vf(i) ∗ df(i)
6:         remainder ← 1 − Sum
7:         if remainder< ϵ then                 ▷ ϵ:very small value
8:             break
9:         else
10:            continue
11:        end if
12:    end for
13:    return
14: end procedure
```

two methods are complementary or reciprocal to each other and ensure that the entire feature space is sampled sufficiently. While the allocation method attempts to find a minimal subset of ODF dimensions that would be non-zero generating a polycrystal solution, the partition method seeks to widen the search across all the 76 dimensions.

VI. Results

In this section, we evaluate the proposed data-driven approach in yielding optimal and near-optimal solutions and find that it outperforms or matches previous state-of-the-art methods and produces numerous near-optimal solutions which is one of the most significant contributions of this study. Table 1 presents the total number of near-optimal solutions, or in other words, solutions that are proximal to the optimal solutions. The near-optimal solutions of this problem correspond to different designs having same or similar values for yield stress. The algorithms were executed to produce around 5 million valid (which obey all the constraints) solutions. It took an average of 112.21 ms and 303.45 ms for generating a valid sample for the partition and the allocation scheme respectively.

Table 1: Number of solutions within 0.01%, 0.1% and 0.5% of the optimal solutions. For each set of constraints (Equations 15a, 16a), 5 million valid data points were generated.

Constraint	Bound	within 0.01%	within 0.1%	within 0.5%
1	Upper	3	89	147
1	Lower	9	92	222
2	Upper	7	402	2015
2	Lower	3	116	1579

Optimization techniques including the methods used by Acar et al. such as a genetic algorithm [16] or linear programming [24] based scheme lead to a unique microstructural solution or sometimes a few. Acar et al. found multiple solutions by augmenting the original solution with null space [24]. Acar and Sundararaghavan [24] previously studied an LP approach to identify the optimal processing routes, which can produce the optimum microstructure designs of the same Galfenol vibration tuning problem. One of the limitations of their approach for vetting equivalent solutions is that it only searches for identical optimal value. However, for practical design applications, a near-optimal solution is adequate as long as the constraints are strictly

obeyed, and the near-optimal solutions are proximal to the optimal solution. For all the four problems (upper and lower bound approaches for two sets of constraints), 3-9 near-optimal solutions with a neighborhood of 10^{-4} (from the optimal solution) are discovered. Further, between 89-402 solutions in a neighborhood of 10^{-3} and between 147-1579 solutions in a neighborhood of $5*10^{-3}$, across all the categories are identified. As described before, obtaining multiple optimal solutions are critical as traditional low-cost manufacturing processes can only generate a limited set of microstructures. While a single solution may not be economically feasible to manufacture, hundreds or thousands of near-optimal solutions can accelerate the speed of materials development. Therefore, it provides flexibility to produce solutions which are cost-effective selectively, and improve the overall efficiency of manufacturing immensely.

Liu et al.'s [25, 51] approach of using guided and generalized pattern search methods was compared with the proposed data-driven methodology for the current design problem. However, neither of these approaches converged to an optimal solution for the current problem. Although both problems have a yielding objective for a cantilevered Galfenol beam, the current problem is more convoluted compared to Liu et al.'s because of additional constraints on the first natural frequencies. Pattern search finds a sequence of points to approach an optimal point. Due to the added constraints in the current problem, pattern search algorithms failed to converge to an optimal solution [60]. For pattern search to successfully reach an optimal solution, it requires a series of valid points at each iteration of the optimization process.

Table 2 illustrates the optimal yield stress values and Young's modulus, shear modulus, bending and torsional frequencies obtained by the proposed method for both sets of constraints and bounds.

Table 2: Summary of the results: The yield stress σ_y, Young's modulus E_1, shear modulus G_{12}, bending ω_{1b} and torsional ω_{1t} frequencies of the optimal solutions generated by the proposed method for both sets of constraints (Equations 15a, 16a)

Constraint	**Bound**	σ_y(in MPa)	E_1(in GPa)	G_{12}(in GPa)	ω_{1b}(in Hz)	ω_{1t}(in Hz)
1	Upper	385.237	209.546	77.313	120.006	21.341
1	Lower	385.113	235.905	82.316	121.272	21.344
2	Upper	388.089	153.160	93.723	102.649	23.497
2	Lower	387.134	184.679	92.772	112.661	23.377

In their previous works [16, 29], Acar et al. used a genetic algorithm based scheme to solve the upper

bound approach. In a later work, Acar et al. [24] converted the upper bound approach to a lower bound approach that involved converting the problem from stiffness domain to compliance (reciprocal of stiffness) domain. Hence, by converting the original problem into a linear problem, Acar et al. arrived at an LP solution for the constrained microstructure design problem. The proposed data-driven approach is compared with the methods advanced by Acar et al. as their approach outperformed other optimization methods. For the upper and lower bound approaches, our solutions are compared against the genetic algorithm based scheme and LP-based methods respectively. The proposed data sampling approach based on the sampling algorithms surpassed the yield stresses obtained from genetic algorithm based solver for the upper bound approach (as shown in Table 3). In particular, we get an improvement of more than 25% for upper bound approach on the first set of objectives against the previous state-of-the art approach. Additionally, the results for the lower bound are comparable to the optimal values achieved by the LP method (Table 4). It is important to note that only the LP solution (used for the lower bound approach by Acar et al. [24]) yields the theoretical maximum value in contrast to the genetic algorithm solver scheme used by them for the upper bound approach [16].

Table 3: Comparison of the maximum yield stress achieved for the 2 sets of constraints with the proposed approach and the previous state-of-the art genetic algorithm solver (GA) [16] approach for microstructure design with process constraints(upper bound). The yield stress σ_y, bending ω_{1b} and torsional ω_{1t} frequencies of the optimal solutions generated by both methods. The units for yield stress σ_y is MPa and the frequencies is Hz.

Constraint	**Bound**	σ_y(current)	σ_y(GA)	ω_{1b}(current)	ω_{1b}(GA)	ω_{1t}(current)	ω_{1t}(GA)
1	Upper	385.237	384.126	120.006	120.210	21.341	21.498
2	Upper	388.089	308.446	102.589	113.918	23.482	23.485

Table 4: Comparison of the maximum yield stress achieved for the 2 sets of constraints with the proposed approach and the previous state-of-the-art LP [24] approach for the microstructure design with process constraints (lower bound). The yield stresses σ_y, bending ω_{1b} and torsional ω_{1t} frequencies of the optimal solutions generated by both methods. The units for the yield stress σ_y is MPa and the frequencies is Hz.

Constraint	**Bound**	σ_y(current)	σ_y(LP)	ω_{1b}(current)	ω_{1b}(LP)	ω_{1t}(current)	ω_{1t}(LP)
1	Lower	385.113	385.650	121.272	120.020	21.344	21.500
2	Lower	387.134	387.259	106.519	100.000	23.477	23.499

Figures 6 and 7 represent the frequency distribution of yield stress values for upper and lower bounds for the first and second set of constraints respectively. Figures 8 and 9 depict the optimal upper and lower bound ODF solutions for the two constraints respectively.

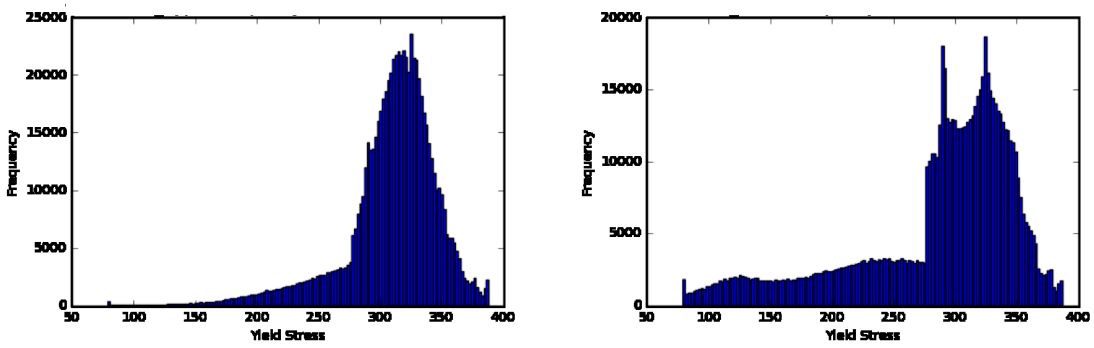

(a) upper bound approach (b) lower bound approach

Fig. 6: Frequency distribution of yield stress values for first set of constraints

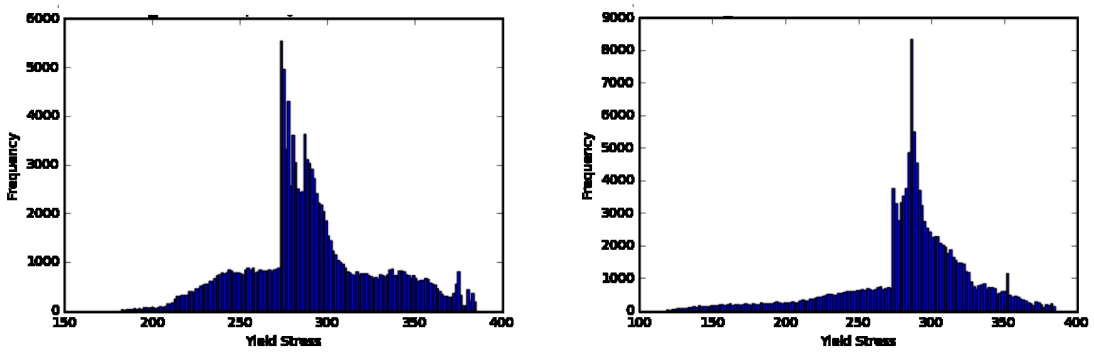

(a) upper bound approach (b) lower bound approach

Fig. 7: Frequency distribution of yield stress values for second set of constraints

A sensitivity analysis is performed by representing the distribution ODF and frequency plot (inset) of the top/highest 1% yield stress values across the 76 ODF dimensions (Figures 10 and 11). The figures exhibit the fraction (or percentage) of non-zero ODFs in the ODF vectors that yield high-stress values, in the case of both upper and lower bound solutions for both sets of constraints. The peaks in the frequency plots represent the ODF dimensions that are non-zero across the majority of ODF vectors yielding the highest objective value (in this case, yield stress). The distribution ODFs in these figures does not exhibit the actual values.

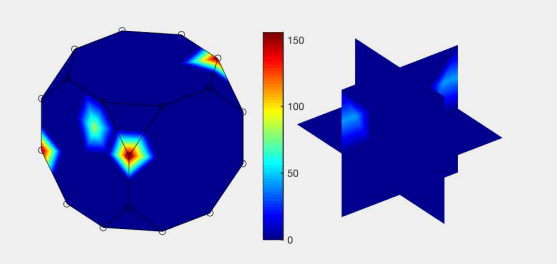

(a) upper bound approach

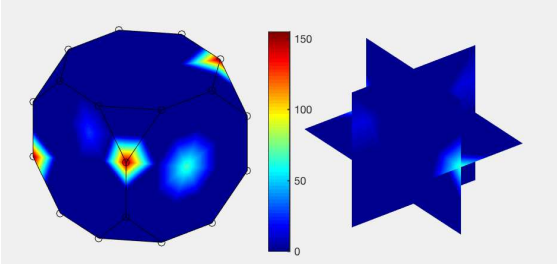

(b) lower bound approach

Fig. 8: Finite element microstructure of optimal ODF examples for the first set of frequency constraints

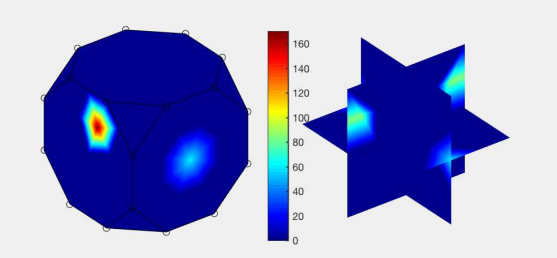

(a) upper bound approach

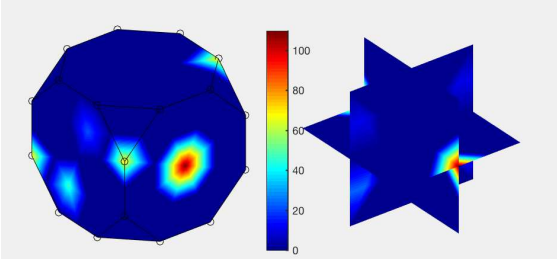

(b) lower bound approach

Fig. 9: Finite element microstructure of optimal ODF examples for the second set of frequency constraints

Rather, they represent the percentage of occurrence of the ODF dimensions in top 1% of the solutions. It is observed that the sensitivity of the near optimum solutions to the ODFs for the lower and upper bound approaches are similar, especially for the first set of constraints. Although the computation of intermediate properties in the case of upper or lower bound solutions is different (stiffness and compliance respectively), this is admissible as the same objective function is being solved. The figures signify that a small number of ODF dimensions can predominantly influence the solution space proximal to the optimal value. This can motivate the development of future sampling approaches for ODF vectors to iteratively adapt to sample across only few ODF dimensions instead of all to accelerate the data-generation process.

One weakness of the proposed data-driven method is its higher time cost compared to LP methods. However, traditional optimization techniques using combinatorial search methods or evolutionary algorithms are also time-consuming. Our framework attempts to search the entire sample space for attaining the optimal or near-optimal solutions. Besides, it should be emphasized that the proposed sampling algorithms are designed to work even for the more difficult problem of nonlinear optimization. Heuristic search using data-driven approaches is beneficial for solving problems in which the objective function has a non-convex

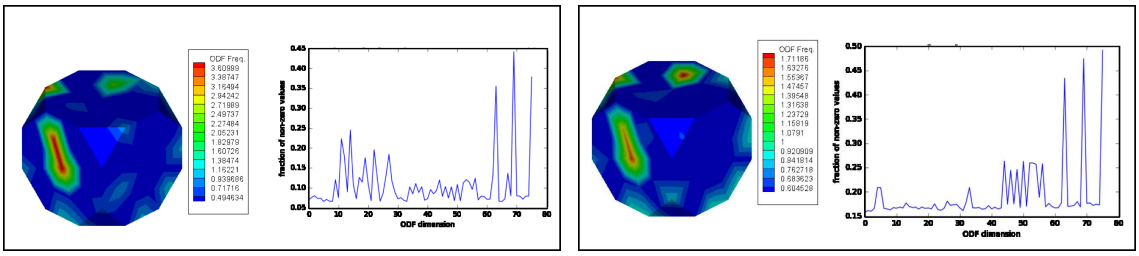

(a) upper bound approach (b) lower bound approach

Fig. 10: Finite element discretized sensitivity plots for ODF and frequency distribution(inset) of the top/highest 1% yield stress values across ODF dimensions for the first set of constraints.

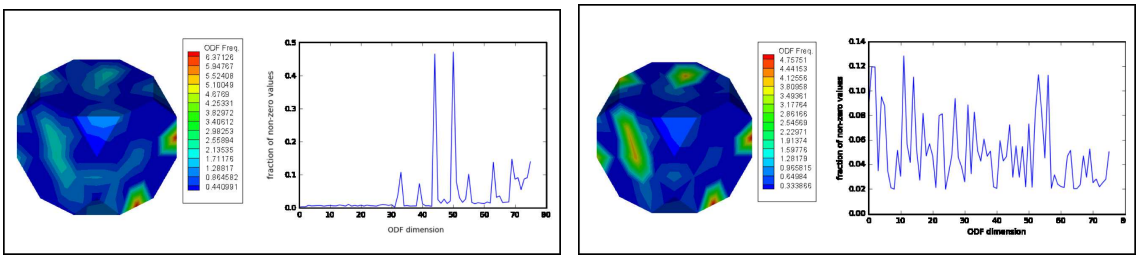

(a) upper bound approach (b) lower bound approach

Fig. 11: Finite element discretized sensitivity plots for ODF and frequency distribution(inset) of the top/highest 1% yield stress values across ODF dimensions for the second set of constraints.

relation to its set of constraints. Another major advantage of the proposed sampling scheme is achieving numerous optimal and near-optimal solutions, that can, in turn, reduce the time and effort for the transition between design and processing.

VII. Conclusion and Future Work

The selection of materials and geometry to maximize or minimize a given property has been a cardinal problem in materials science. The potential of data-driven approaches for solving a constrained microstructure design problem for both upper and lower bound methods is expounded by the proposed strategy. Our approach arrives at a higher (or in few cases, equivalent) optimal value than the previous state-of-the-art methods. The data generation strategies attempt to explore the entire sample space and generate numerous near-optimal solutions (about 100-1000, i.e. $2-3$ orders of magnitude more than prior methods). Previous approaches including LP techniques lead to a unique or a handful of optimal solutions. Numerous near-optimal solutions give the flexibility to use traditional low-cost manufacturing processes such as forming and heat treatment.

These processes can generate only a limited set of microstructures, and frequently manufacturing from a single optimal solution may not be feasible.

Leveraging data-driven techniques can play an essential role in the expedition of a precise design of materials with process constraints. This study has demonstrated the power of carefully designed sampling approaches by identifying multiple near-optimal solutions for a non-linear optimization problem, and is expected to inspire the development of alternative sampling schemes building upon the ones proposed in this work which can reach optimal solutions faster and deliver numerous near-optimal solutions. Further, with parallel computing technologies becoming inexpensive, especially Graphical Processing Units(GPU) computing, distributed implementations of our algorithm can significantly diminish the optimization time. The proposed approach for maximizing the yield stress under process constraints using data sampling algorithms can be extended for property optimizations for other non-linear design limitations and other materials. The sampling schemes are generalizable and agnostic of the problem domain and can be used in other scientific domains as well.

The analysis for the constrained microstructure optimization problem depicts that certain combinations of ODF dimensions are non-zero more often in the ODF vector of the near-optimal solutions. The proposed work provides a future direction for feedback aware sampling that can iteratively incentivize distinct ODF dimensions that yield ODF vectors with higher objective value, which can be investigated to accelerate the process of attaining optimal or near-optimal solutions.

Appendix: More Optimal ODF Solutions

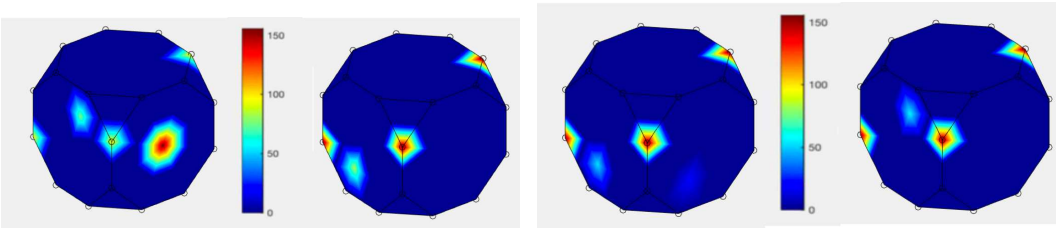

(a) upper bound solution (b) lower bound solution

Fig. 12: More finite element microstructure examples of near-optimal ODF solutions for the first set of constraints

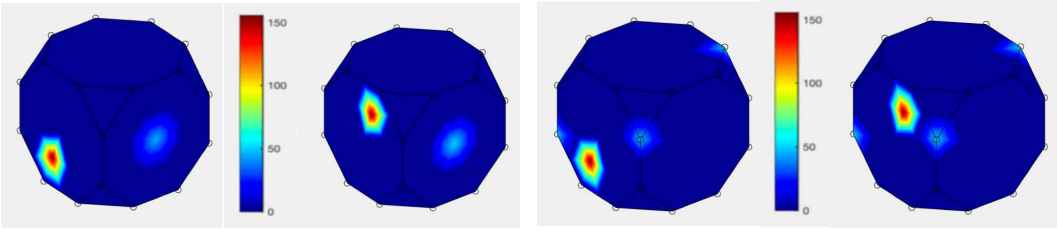

(a) upper bound solution (b) lower bound solution

Fig. 13: More finite element microstructure examples of near-optimal ODF solutions for the second set of constraints

Acknowledgments

This work is supported primarily by the AFOSR MURI award FA9550-12-1-0458. Partial support is also acknowledged from the following grants: NIST award 70NANB14H012; NSF award CCF-1409601; DOE awards DE-SC0007456, DE-SC0014330; and Northwestern Data Science Initiative.

References

[1] G. B. Olson, Science **277**, 1237 (1997), doi: 10.1126/science.277.5330.1237.

[2] A. Agrawal and A. Choudhary, APL Materials **4**, 053208 (2016), doi: 10.1063/1.4946894.

[3] V. Sundararaghavan and N. Zabaras, Acta Materialia **55**, 1573 (2007), doi: 10.1016/j.actamat.2006.10.019.

[4] A. Agrawal, P. D. Deshpande, A. Cecen, G. P. Basavarsu, A. N. Choudhary, and S. R. Kalidindi, Integrating Materials and Manufacturing Innovation **3**, 1 (2014), doi: 10.1186/2193-9772-3-8.

[5] L. Ward, A. Agrawal, A. Choudhary, and C. Wolverton, npj Computational Materials **2**, 16028 (2016), doi: 10.1038/npjcompumats.2016.28.

[6] R. Liu, Y. C. Yabansu, Z. Yang, A. N. Choudhary, S. R. Kalidindi, and A. Agrawal, Integrating Materials and Manufacturing Innovation , 1 (2017), doi: 10.1007/s40192-017-0094-3.

[7] P. Deshpande, B. Gautham, A. Cecen, S. Kalidindi, A. Agrawal, and A. Choudhary, in *Proceedings of the 2nd World Congress on Integrated Computational Materials Engineering (ICME)* (Springer, 2013) pp. 155–160, doi: 10.1002/9781118767061.ch25.

[8] R. Liu, A. Agrawal, W.-k. Liao, A. Choudhary, and M. De Graef, in *Big Data (Big Data), 2016 IEEE International Conference on* (IEEE, 2016) pp. 2261–2269, doi: 10.1109/BigData.2016.7840857.

[9] B. Meredig, A. Agrawal, S. Kirklin, J. E. Saal, J. Doak, A. Thompson, K. Zhang, A. Choudhary, and C. Wolverton, Physical Review B **89**, 094104 (2014), doi: 10.1103/PhysRevB.89.094104.

[10] R. Liu, Y. C. Yabansu, A. Agrawal, S. R. Kalidindi, and A. N. Choudhary, Integrating Materials and Manufacturing Innovation **4**, 13 (2015), doi: 10.1186/s40192-015-0042-z.

[11] A.-G. Olabi and A. Grunwald, Materials & Design **29**, 469 (2008), doi: 10.1016/j.matdes.2006.12.016.

[12] R. Grossinger, R. S. Turtelli, and N. Mehmood, in *IOP Conference Series: Materials Science and Engineering*, Vol. 60 (IOP Publishing, 2014) p. 012002, doi: 10.1088/1757-899X/60/1/012002.

[13] F. Claeyssen, N. Lhermet, R. Le Letty, and P. Bouchilloux, Journal of alloys and compounds **258**, 61 (1997), doi: 10.1016/S0925-8388(97)00070-4.

[14] H. Zhang, T. Zhang, and C. Jiang, Smart Materials and Structures **22**, 115009 (2013), doi: 10.1088/0964-1726/22/11/115009.

[15] Y. Yamamoto, H. Eda, and J. Shimizu, in *Advanced Intelligent Mechatronics, 1999. Proceedings. 1999 IEEE/ASME International Conference on* (IEEE, 1999) pp. 215–220, doi: 10.1109/AIM.1999.803169.

[16] P. Acar and V. Sundararaghavan, in *57th AIAA/ASCE/AHS/ASC Structures, Structural Dynamics, and Materials Conference* (2016) p. 0156, doi: 10.2514/6.2016-0156.

[17] A. Kumar and V. Sundararaghavan, Finite Elements in Analysis and Design **127**, 1 (2017), doi: 10.1016/j.finel.2016.11.009.

[18] R. Kellogg, A. Russell, T. Lograsso, A. Flatau, A. Clark, and M. Wun-Fogle, Acta Materialia **52**, 5043 (2004), doi: 10.1016/j.actamat.2004.07.007.

[19] J. Restorff, M. Wun-Fogle, and A. Clark, Journal of Applied Physics **103**, 07B305 (2008), doi: 10.1063/1.2832667.

[20] A. Mahadevan, P. Evans, and M. Dapino, Applied Physics Letters **96**, 012502 (2010), doi: 10.1063/1.3280374.

[21] L. M. Cheng, A. E. Nolting, B. Voyzelle, and C. Galvani, Behavior and Mechanics of Multifunctional and Composite Materials, Edited by Dapino, Marcelo J.. Proceedings of the SPIE **6526**, 65262N (2007), doi: 10.1117/12.720664.

[22] S.-M. Na and A. B. Flatau, Journal of Applied Physics **103**, 07D304 (2008), doi: 10.1063/1.2838772.

[23] N. Srisukhumbowornchai and S. Guruswamy, Metallurgical and Materials Transactions A **35**, 2963 (2004), doi: 10.1007/s11661-004-0243-0.

[24] P. Acar and V. Sundararaghavan, AIAA Journal **54**, 4022 (2016), doi: 10.2514/1.J055247.

[25] R. Liu, A. Kumar, Z. Chen, A. Agrawal, V. Sundararaghavan, and A. Choudhary, Scientific reports **5** (2015), doi: 10.1038/srep11551.

[26] B. L. Adams, A. Henrie, B. Henrie, M. Lyon, S. Kalidindi, and H. Garmestani, Journal of the Mechanics and Physics of Solids **49**, 1639 (2001), doi: 10.1016/S0022-5096(01)00016-3.

[27] S. R. Kalidindi, J. R. Houskamp, M. Lyons, and B. L. Adams, International Journal of Plasticity **20**, 1561 (2004), doi: 10.1016/j.ijplas.2003.11.007.

[28] T. Fast, M. Knezevic, and S. R. Kalidindi, Computational Materials Science **43**, 374 (2008), doi: 10.1016/j.commatsci.2007.12.002.

[29] P. Acar and V. Sundararaghavan, AIAA Journal **54**, 1751 (2016), doi: 10.2514/1.J054822.

[30] S.-M. Na and A. B. Flatau, Journal of applied physics **101**, 09N518 (2007), doi: 10.1063/1.2712822.

[31] H.-J. Bunge, *Texture analysis in materials science: mathematical methods* (Elsevier, 2013).

[32] A. Heinz and P. Neumann, Acta Crystallographica Section A: Foundations of Crystallography **47**, 780 (1991), doi: 10.1107/S0108767391006864.

[33] U. F. Kocks, C. N. Tomé, and H.-R. Wenk, *Texture and anisotropy: preferred orientations in polycrystals and their effect on materials properties* (Cambridge university press, 2000).

[34] V. Randle and O. Engler, *Introduction to texture analysis: macrotexture, microtexture and orientation mapping* (CRC press, 2000).

[35] A. Kumar and P. Dawson, Acta Materialia **48**, 2719 (2000), doi: 10.1016/S1359-6454(00)00044-6.

[36] G. I. Taylor, Stephen Timoshenko 60th Anniversary Volume , 218 (1938), doi: 10.1016/0022-5096(57)90058-3.

[37] D. Chung and W. Buessem, Journal of Applied Physics **38**, 2010 (1967), doi: 10.1063/1.4962996.

[38] H. Wang, Y. Zhang, R. Wu, L. Sun, D. Xu, and Z. Zhang, Scientific reports **3** (2013), doi: 10.1038/srep03521.

[39] R. Shi, N. Zhou, S. Niezgoda, and Y. Wang, Acta Materialia **94**, 224 (2015), doi: 10.1016/j.actamat.2015.04.050.

[40] P. Weetman and G. Akhras, Journal of Applied Physics **114**, 183911 (2013), doi: 10.1063/1.4831666.

[41] A. Boesenberg, J. Restorff, M. Wun-Fogle, H. Sailsbury, and E. Summers, Journal of Applied Physics **113**, 17A909 (2013), doi: 10.1063/1.4794186.

[42] J. Domann, C. Loeffler, B. Martin, and G. Carman, Journal of Applied Physics **118**, 123904 (2015), doi: 10.1063/1.4930891.

[43] H. Cao, P. M. Gehring, C. Devreugd, J. Rodriguez-Rivera, J. Li, and D. Viehland, Physical review letters **102**, 127201 (2009), doi: 10.1103/PhysRevLett.102.127201.

[44] R. A. Kellogg, *Development and modeling of iron-gallium alloys*, Ph.D. thesis, Iowa State University (2003).

[45] A. Clark, M. Wun-Fogle, J. Restorff, and T. Lograsso, in *Proc. of Pacific Rim International Conference on Advanced Materials and Processing*, Vol. 11 (Honolulu, HI, Dec, 2001).

[46] E. M. Summers, T. A. Lograsso, J. D. Snodgrass, and J. C. Slaughter, in *Smart Structures and Materials* (International Society for Optics and Photonics, 2004) pp. 448–459, doi: 10.1117/12.539781.

[47] A. E. Clark, J. B. Restorff, M. Wun-Fogle, T. A. Lograsso, and D. L. Schlagel, IEEE Transactions on Magnetics **36**, 3238 (2000), doi: 10.1109/20.908752.

[48] A. E. Clark, M. Wun-Fogle, J. B. Restorff, and T. A. Lograsso, Materials Transactions **43**, 881 (2002), doi: 10.2320/matertrans.43.881.

[49] R. Kellogg, A. B. Flatau, A. Clark, M. Wun-Fogle, and T. A. Lograsso, Journal of applied physics **91**, 7821 (2002), doi: 10.1063/1.1452216.

[50] T. Ueno, E. Summers, and T. Higuchi, Sensors and Actuators A: Physical **137**, 134 (2007), doi: 10.1016/j.sna.2007.02.026.

[51] R. Liu, A. Agrawal, W.-k. Liao, A. Choudhary, and Z. Chen, in *Contemporary Computing (IC3), 2015 Eighth International Conference on* (IEEE, 2015) pp. 13–18, doi: 10.1109/IC3.2015.7346645.

[52] R. M. Lewis and V. Torczon, SIAM Journal on Optimization **9**, 1082 (1999), doi: 10.1137/S1052623496300507.

[53] R. M. Lewis and V. Torczon, SIAM Journal on Optimization **10**, 917 (2000), doi: 10.1137/S1052623497331373.

[54] C. Audet and J. E. Dennis Jr, SIAM Journal on Optimization **13**, 889 (2002), doi: 10.1137/S1052623400378742.

[55] C. Audet and J. E. Dennis Jr, SIAM Journal on Optimization **14**, 980 (2004), doi: 10.1137/S105262340138983X.

[56] E. Rigoni and A. Turco, in *Asia-Pacific Conference on Simulated Evolution and Learning* (Springer, 2010) pp. 523–532, doi: 10.1007/978-3-642-17298-4_56.

[57] J. Gondzio and T. Terlaky, Advances in Linear and Integer Programming. Oxford University Press: Oxford , 103 (1996).

[58] P. Downey and A. Flatau, Journal of Applied Physics **97**, 10R505 (2005), doi: 10.1063/1.1853838.

[59] S. Datta and A. B. Flatau, in *MRS Proceedings*, Vol. 888 (Cambridge Univ Press, 2005) pp. 0888–V04, doi: 10.1557/PROC-0888-V04-09.

[60] V. Torczon, SIAM Journal on optimization **7**, 1 (1997), doi: 10.1137/S1052623493250780.